Received: 20 June 2016 | Accepted: 07 November 2016

DOI: 10.1111/gbi.12221

ORIGINAL ARTICLE

WILEY gebiology

Geochemically distinct carbon isotope distributions in *Allochromatium vinosum* DSM 180^T grown photoautotrophically and photoheterotrophically

T. Tang[1,2] | **W. Mohr**[1,3] | **S. R. Sattin**[1] | **D. R. Rogers**[4,5] | **P. R. Girguis**[4] | **A. Pearson**[1]

[1]Department of Earth and Planetary Sciences, Harvard University, Cambridge, MA, USA

[2]State Key Laboratory of Marine Environmental Science, Xiamen University, Xiamen, China

[3]Department of Biogeochemistry, Max Planck Institute for Marine Microbiology, Bremen, Germany

[4]Department of Organismic and Evolutionary Biology, Harvard University, Cambridge, MA, USA

[5]Department of Chemistry, Stonehill College, Easton, MA, USA

Correspondence
T. Tang and A. Pearson, Department of Earth and Planetary Sciences, Harvard University, Cambridge, MA, USA.
Emails: pearson@eps.harvard.edu and tiantian.tang@xmu.edu.cn

Funding information
Gordon and Betty Moore Foundation; NSF-DEB Dimensions of Biodiversity Program; Marie Curie International Outgoing Fellowship

Abstract

Anoxygenic, photosynthetic bacteria are common at redox boundaries. They are of interest in microbial ecology and geosciences through their role in linking the carbon, sulfur, and iron cycles, yet much remains unknown about how their flexible carbon metabolism—permitting either autotrophic or heterotrophic growth—is recorded in the bulk sedimentary and lipid biomarker records. Here, we investigated patterns of carbon isotope fractionation in a model photosynthetic sulfur-oxidizing bacterium, *Allochromatium vinosum* DSM180^T. In one treatment, *A. vinosum* was grown with CO_2 as the sole carbon source, while in a second treatment, it was grown on acetate. Different intracellular isotope patterns were observed for fatty acids, phytol, individual amino acids, intact proteins, and total RNA between the two experiments. Photoautotrophic CO_2 fixation yielded typical isotopic ordering for the lipid biomarkers: $\delta^{13}C$ values of phytol > *n*-alkyl lipids. In contrast, growth on acetate greatly suppressed intracellular isotopic heterogeneity across all molecular classes, except for a marked ^{13}C-depletion in phytol. This caused isotopic "inversion" in the lipids ($\delta^{13}C$ values of phytol < *n*-alkyl lipids). The finding suggests that inverse $\delta^{13}C$ patterns of *n*-alkanes and pristane/phytane in the geologic record may be at least in part a signal for photoheterotrophy. In both experimental scenarios, the relative isotope distributions could be predicted from an isotope flux-balance model, demonstrating that microbial carbon metabolisms can be interrogated by combining compound-specific stable isotope analysis with metabolic modeling. Isotopic differences among molecular classes may be a means of fingerprinting microbial carbon metabolism, both in the modern environment and the geologic record.

1 | INTRODUCTION

The contribution of anoxygenic photosynthesis to the carbon cycle is linked to the magnitude and geochemical impact of the sulfur and iron cycles, and both are important factors in understanding Earth's transition from the lower-oxygen Proterozoic to the higher-oxygen Phanerozoic (Johnston, Wolfe-Simon, Pearson, & Knoll, 2009). While ferruginous conditions are thought to dominate in low-nutrient anoxic systems (Canfield, 1998), euxinia reigns in productive environments (Overmann, Beatty, Hall, Pfennig, & Northcote, 1991; Schunck et al., 2013) or in locations where free sulfide from pore waters or bottom waters intersects with phototrophic microbial mats (Meyer et al., 2011; Voorhies et al., 2012). In such environments, microbial photosynthesis ultimately preserves a rich organic geochemical record (Brocks et al., 2005; French, Sepulveda, Trabucho-Alexandre, Groceke, & Summons, 2014; Grice et al., 2005; Johnston et al., 2010; Meyer & Kump, 2008;

Pancost et al., 2004). However, the balance of microbial carbon input to the total preserved organic matter or to the lipid biomarker record remains difficult to interpret.

Photosynthetic micro-organisms use a variety of pathways to fix carbon. Most common is the Calvin–Benson–Bassham (CBB) cycle (Calvin & Benson, 1948), in which the primary CO_2-fixing enzyme is ribulose-bisphosphate carboxylase oxygenase (Rubisco). Alternatively, some taxa use the reverse tricarboxylic acid (rTCA) pathway to fix carbon via the carboxylases of central metabolism (Evans, Buchanan, & Arnon, 1966). Most critically, many CBB-pathway phototrophs also are capable of heterotrophy and/or mixotrophy, assimilating organic carbon substrates in addition to or instead of fixing CO_2 (Bryant et al., 2012; Madigan & Jung, 2009). Such species, which includes all sulfur oxidizers and many cyanobacteria (Michelou, Cottrell, & Kirchman, 2007), may express their flexible carbon metabolisms differently depending on environmental growth conditions, ultimately affecting the record of carbon preservation.

Although the relative contribution of microbial carbon fixation by the CBB-pathway relative to rTCA and other enzymatic pathways remains uncertain in some settings (Campbell, Engel, Porter, & Takai, 2006; Hanson, Alber, & Tabita, 2012; Luo et al., 2014; Van Der Meer, Schouten, De Leeuw, & Ward, 2000), in general, the total organic carbon (TOC) isotope record of the Proterozoic and Phanerozoic is consistent with dominance of the CBB cycle through most of Earth history (Hayes, Strauss, & Kaufman, 1999). The bulk $\delta^{13}C_{TOC}$ record of a CBB-driven ecosystem includes all sources that produce and assimilate this carbon, including both oxygenic and anoxygenic phototrophs, and heterotrophic consumers. As a result, the relative importance not only of these functional groups, but also more generally of algal versus microbial, photic versus aphotic, and planktonic versus benthic carbon contributions can be challenging to decipher from the sedimentary record and may have fluctuated through time (Damste & Schouten, 1997; Des Marais, Strauss, Summons, & Hayes, 1992).

In parallel with questions about the variability of bulk organic matter sources, lipid biomarkers from the Proterozoic and Phanerozoic show different patterns of carbon isotope distribution. Pristane and phytane are diagenetic hydrocarbon products of phytol, the esterified side chain of chlorophyll, and thus are attributable to photosynthetic organisms. Straight chain, or *n*-alkyl, lipids are membrane hydrocarbon components of all bacteria and eukaryotes, both autotrophic and heterotrophic. In sediments of the Proterozoic—and especially in Ediacaran records—pristane and phytane are depleted in ^{13}C relative to *n*-alkyl lipids. This pattern represents an inversion of normal isotopic signatures, and it largely disappears from the sedimentary record near the Cambrian boundary (Kelly, Love, Zumberge, & Summons, 2011; Logan, Hayes, Hieshima, & Summons, 1995; Logan, Summons, & Hayes, 1997), although it returns episodically in the Paleozoic (Grice, Schaeffer, Schwark, & Maxwell, 1996; Grice et al., 2005; Guthrie, 1996; Joachimski et al., 2001; Nabbefeld et al., 2010; Schwab & Spangenberg, 2004).

Such a pattern is "inverse" to normal biosynthetic expectations (Hayes, 2001), because in photosynthetic taxa fixing carbon by the CBB pathway, phytol (the precursor to pristane and phytane) is ^{13}C-enriched relative to fatty acids (FAs) by ca. 2–4‰ (Jahnke et al., 2004; Sakata et al., 1997; Schouten et al., 1998). This relationship holds both for organisms that use the mevalonic acid (MVA) pathway for isoprenoid synthesis, as well as for taxa that use the alternative methylerythritol phosphate (MEP) pathway (Hayes, 2001; Rohmer, Knani, Simonin, Sutter, & Sahm, 1993). Photosynthetic biomass synthesized according to the standard CBB paradigm cannot have relatively ^{13}C-poor phytol as is seen commonly in Proterozoic rocks.

Explanations for the "inverse" pattern most often invoke the presence of anomalously ^{13}C-enriched *n*-alkyl material relative to a primary pristane/phytane source (Logan et al., 1995). Values of $\delta^{13}C$ for *n*-alkyl lipids from the Ediacaran are on average 1.5‰ more positive than the kerogen from which they are extracted (Logan et al., 1995, 1997) and have been attributed to heterotrophic bacteria. This explanation is invoked by analogy to the ^{13}C-enrichment in eukaryotic heterotrophs that is caused by preferential loss of $^{12}CO_2$ during respiration (Deniro & Epstein, 1978). Recent modeling exercises, however, have questioned whether microbial systems could sustain enough trophic depth to generate a sufficiently large isotope effect, suggesting that additional processes are needed (Close, Bovee, & Pearson, 2011).

One possibility is that patterns of intracellular carbon isotope distribution may be more flexible in phototrophic, CBB-utilizing microbial taxa than is presently recognized. To date, these patterns, both for lipids and for other biomolecular classes, are assumed to conform to a single pattern: $\delta^{13}C_{sugar} > \delta^{13}C_{protein} \approx \delta^{13}C_{biomass} > \delta^{13}C_{Phytol} > \delta^{13}C_{n\text{-}alkyl}$ (Hayes, 2001). Patterns that deviate from this order are assumed to require alternative pathways of carbon fixation other than the CBB cycle and reflect the use of different enzymes for intracellular biosynthetic processes (e.g., rTCA in the *Epsilonproteobacteria* or the 3-hydroxypropionate pathway in the *Chloroflexi*; Van Der Meer, Schouten, & Damste, 1998; Van Der Meer et al., 2001). More studies are needed for bacteria that employ flexible carbon metabolisms, including CBB-cycle taxa that can grow heterotrophically or by mixotrophy. Understanding the biological underpinning of intracellular carbon isotope patterns helps illuminate the corresponding record in ancient sediments. Although the full suite of biomolecules is lost, rocks preserve isotopic signatures of macromolecular materials and bulk biomass (in kerogen) and of lipids (in bitumen).

To address this issue, here we conducted two chemostat-controlled growth studies of the model phototroph, *Allochromatium vinosum* DSM 180^T. The *Chromatiaceae* are believed to play a major role in anoxygenic photosynthesis in the environment, leaving biomarker evidence of photic zone euxinia via the carotenoid lipid, okenone (Brocks et al., 2005; French, Rocher, Zumberge, & Summons, 2015). *Allochromatium vinosum* is metabolically versatile, with phototrophic growth possible on CO_2, malate, acetate, and other low molecular weight organic acids (Imhoff, 2005); it will even grow chemoautotrophically in the dark (Kampf & Pfennig, 1980). Recent work on its genome, proteome, and metabolome establishes a strong base of complementary information (Weissgerber, Sylvester, Kroninger, & Dahl, 2014; Weissgerber, Watanabe, Hoefgen, & Dahl, 2014; Weissgerber et al., 2011). By employing continuous-culture conditions, rather than a series of batch cultures, we ensured that all biomass samples for the various analyses

were taken at steady state and that the cells were metabolically stable. The results provide a frame of reference for parallel "–omics" studies, yielding metabolic insights: Namely, we show that the resulting intracellular patterns of ^{13}C distribution are predictable, influenced strongly by the mode of carbon incorporation, and distinct in the geologically preservable lipids.

2 | MATERIALS AND METHODS

2.1 | Bacterial strain, chemostat setup, and monitoring

A stirred 8-L culture of *A. vinosum* DSM 180^T was grown anaerobically in a 10-L bioreactor with continuous medium (4.3L/day) and 10% CO_2 in N_2 controlled by a BIOSTAT® B plus integrated system (Sartorius, Germany). The CO_2 was from a cylinder with known $\delta^{13}C$ value of −37.1‰. pH was controlled at 7.5 by an auto-balancing program that injected 1 N HCl or 1 N NaOH as needed. Redox potential, pH, temperature, and optical density were monitored throughout the incubations, with periodic external calibration of the sensors (Fig. S1). Light intensity was ca. 5 µmol quanta m^{-2} s^{-1}. Culture outflow was collected in sterile glass bottles at 4°C. The culture was grown in two modes. In autotrophic mode, it was grown photolithoautotrophically in medium containing 6.4 mM NH_4Cl, 4.6 mM KCl, 2.5 mM HEPES, 2.5 mM $MgCl_2$, 1.7 mM $CaCl_2$, 1 mM KH_2PO_4, SL12B trace metals, and vitamin B_{12}. Sodium sulfide (1.3 mM) was added continuously as the electron donor by gas-tight syringe pump to maintain a redox potential below −200 mV. In heterotrophic mode, the culture was grown photoorganoheterotrophically with the addition of 15 mM sodium acetate with known $\delta^{13}C$ content of −46.0‰ as the carbon source. Sodium thiosulfate (4.0 mM) was added as the reducing agent instead of sodium sulfide, and the gas flow was changed to 100% N_2. Culture outflow was harvested daily by centrifugation (4,000 *g*, 15 min), and cell pellets were stored at −20°C (for isotopes) or −80°C (for proteomics). Dissolved inorganic carbon (DIC) concentration, $\delta^{13}C$ of biomass, optical density, and particulate organic carbon also were monitored daily.

2.2 | Bulk $\delta^{13}C$ analysis of cells

Bulk values of $\delta^{13}C$ were measured in two ways. Aliquots of harvested cell pellets were acidified with 1 N HCl to remove DIC, dried in a tin capsule (Costech), and analyzed by elemental analyzer (EA)-IRMS (Stable Isotope Laboratory, http://www.mbl.edu/ecosystems/silab/). Separately, pellets from 1 ml of culture were washed with 50 mM NaCl, centrifuged at 4,000 *g*, and resuspended; 1 µl of this concentrated cell culture was analyzed by spooling-wire microcombustion-IRMS (SWiM-IRMS; Mohr, Tang, Sattin, Bovee, & Pearson, 2014; Sessions, Sylva, & Hayes, 2005).

2.3 | Compound-specific $\delta^{13}C$ analysis—amino acids

Cell pellets (25 mg) were washed with 50 mM NaCl and resuspended with 6 N HCl in Pyrex culture tubes. Norleucine (Sigma-Aldrich) was added as internal standard. After purging under N_2, the samples were hydrolyzed at 110°C for 20 hr and then dried under N_2 at 65°C. Hydrolysates were dissolved in 0.01 N HCl, filtered through 0.2-µm Acrodisc syringe filters and redried. Amino acids (AAs) were derivatized following a modified method from Silfer, Engel, Macko, and Jumeau (1991). Dried hydrolysate was esterified with acidified (20% acetyl chloride) isopropanol at 110°C for 1 hr. Esterification was terminated by chilling, and solvent was removed with N_2 at 0°C followed by rinses with CH_2Cl_2. The esterified samples were then acylated with 25% trifluoroacetic anhydride (Sigma-Aldrich) in CH_2Cl_2 at 100°C for 15 min, dried, and dissolved in ethyl acetate. A mixed standard of 15 AAs (Sigma-Aldrich) was prepared in parallel through the esterification and acylation. Individual AAs were identified and quantified by Agilent 6890N gas chromatograph with a 30 × 0.25 mm Agilent DB-5MS column coupled to an Agilent 5973 mass spectrometer (GC-MS; Table S1). Isotope analysis was performed by gas chromatography–isotope ratio mass spectrometry (GC-IRMS; Thermo Delta V Advantage connected to a Trace GC Ultra via a GC Isolink interface; 30 m × 0.25 mm, HP-5MS column). Each sample was measured in triplicate. Corrections for carbon added during derivatization were calculated using the mixed AA standards analyzed in parallel. Eleven AAs were chromatographically resolved by GC-IRMS: Ala, Gly, Thr, Leu, Ile, Pro, Asx (Asp + Asn), Glx (Glu + Gln), Phe, Lys, and Tyr; Ser and Val were suspected to have co-eluted and could not be reported.

2.4 | Compound-specific $\delta^{13}C$ analysis—lipids

Lipids were extracted from centrifuged cell pellets (Bligh & Dyer, 1959), and the total lipid extract was further separated over SiO_2 gel (Close, Wakeham, & Pearson, 2014), eluting glycolipids in 75% ethyl acetate/25% methanol (v/v) and phospholipids in 100% methanol. Glycolipids and phospholipids were transesterified to FA methyl esters (FAMEs; 5% HCl/methanol (v/v), 70°C, 4 hr) and extracted into hexane/CH_2Cl_2 (9:1, v/v). FAME derivatives of *n*-$C_{16:0}$, *n*-$C_{19:0}$, and *n*-$C_{24:0}$ FA standards with known $\delta^{13}C$ were prepared in parallel to correct for the ^{13}C content of the derivative carbon introduced during transesterification. FAMEs were identified on the same GC-MS as for AAs. For analysis of phytol, centrifuged cell pellets were hydrolyzed in 0.5 N KOH in methanol (70°C, 3 hr), then the base lysates were extracted and separated over SiO_2 gel as described above. Alcohol fractions were derivatized to acetates (acetic anhydride/pyridine, 1:1), along with external standards of *n*-C_{19}–OH and stigmasterol (Aldrich). FAME and phytol $\delta^{13}C$ values (Fig. S2) were determined by GC-IRMS, as described for AAs.

2.5 | Protein stable isotope fingerprinting

The $\delta^{13}C$ values of individual proteins were measured by protein stable isotope fingerprinting (P-SIF; Mohr et al., 2014). Briefly, proteins were extracted from cell pellets by sonication in B-PER protein extraction reagent (Thermo Scientific). After centrifugation at 16,000 *g*, proteins were precipitated from the

supernatant in acetone, then resuspended in 100 mM NH_4HCO_3, pH 9. Multidimensional protein chromatography was used to separate each extract into 960 fractions: first by strong anion exchange (Agilent PL-SAX column; 4.6 × 50 mm, 8 μm) on an Agilent 1100 series HPLC with DAD detector and fraction collector (20 fractions), then by reverse phase (Agilent Poroshell 300SB-C3 column, 2.1 × 75 mm, 5 μm; 48 fractions). Fractions are split into 96-well plates, with 70% of each fraction for isotope analysis and 30% retained for tryptic digestion and peptide sequencing. Plates for isotope analysis were dried by centrifugal vacuum evaporation and then resuspended with the help of a mild Fenton oxidation and UV radiation. Values of $\delta^{13}C$ were measured by SWiM-IRMS with automated injections (Fig. S3).

2.6 | Nucleic acid $\delta^{13}C$ analysis

Cell pellets were washed in 50 mM NaCl, centrifuged (12,000 *g*), and extracted using an Ambion PureLink RNA Mini Kit according to manufacturer's instructions. RNA was recovered in RNAse-free H_2O. To remove residual carbon from extraction buffers, samples were further cleaned by reprecipitation methods developed specifically for $\delta^{13}C$ analysis of RNA (Pearson, Sessions, Edwards, & Hayes, 2004; Pearson et al., 2008). RNA was resuspended in H_2O and analyzed by SWiM-IRMS.

2.7 | Proteomics

Protein stable isotope fingerprinting plates were alkylated with iodoacetamide and digested with trypsin (overnight, 37°C; Mohr et al., 2014). Digests were dried by vacuum centrifugation, resuspended in H_2O with 2% acetonitrile, 0.1% formic acid, and identified by capillary LC-MS/MS using an Agilent 1200 Series HPLC (Kinetex C_{18} column; 2.1 × 100 mm, 2.6 μm in particle size) and an Agilent 6520 quadrupole time-of-flight mass spectrometer (QToF-MS/MS). Bulk protein extracts for comprehensive proteomics were similarly digested with trypsin, then separated into fractions on an Agilent 1200 Series HPLC, followed by analysis on a Thermo Scientific LTQ Velos Orbitrap Mass Spectrometer (3 μm trap column, 5 μm analytical C_{18} column). Peptides were identified in SpectrumMill (Agilent Rev.A.03.03.084 SR 4) by searching all MS^2 spectra against databases of predicted proteins for *A. vinosum* DSM 180^T downloaded from NCBI (http://www.ncbi.nlm.nih.gov/). Ion abundance data were normalized to *z*-scores and matched to the KEGG Orthology (Weissgerber et al., 2011; Table S2). Clustering was performed in Matlab R2015b.

2.8 | Isotope flux-balance model

A cellular isotope mass balance model (Hayes, 2001) of coupled, first-order differential equations was solved to steady state in Matlab R2015b using Monte Carlo resampling approaches (randsample) and the ode23 integrator. In addition to carbon incorporation from acetate and CO_2, the model contains modules for the TCA cycle, anaplerotic reactions (phosphoenolpyruvate carboxylase [PEPC]; and phosphoenolpyruvate carboxykinase [PEPCK]), and other internal carboxylations (malic enzyme [ME]; pyruvate synthase [PS]). All enzymatic processes included in the model were detected in the expressed proteome.

The model has 23 internal metabolite fluxes (φ_{1-23}), seven output fluxes to generate the molecular classes that collectively yield "biomass" (φ_{24-30}), and two substrate exchange loops that allow for isomerization and isotopic homogenization (φ_{31-34}; Tables S3 and S4). Consensus values for the proportions of biomass output (φ_{24-30}) were determined from the measured AA compositions (Table S1), typical lipid yields of 10%–15% of biomass, and the metabolite abundances determined by Weissgerber, Watanabe, et al. (2014) for similar experiments. Given these known product ratios and the fixed stoichiometry of the intracellular reaction network, the only degrees of freedom are the relative fluxes through network branch points. There are four such constraints (unknowns) that must be imposed to solve the model: three internal branch points (*C*, isocitrate lyase; *K*, PEPCK vs. PEPC; and φ_5, the magnitude and direction of carbon flow between pyruvate and PEP), plus the net biomass (*B*, biomass produced vs. CO_2 respired). All other fluxes are governed by stoichiometric dependence. To run the model in autotrophic mode ($\varphi_2 \equiv 1$), we assumed no acetate uptake ($\varphi_1 \equiv 0$); the converse was assumed when modeling acetate assimilation.

The model additionally requires that kinetic isotope effects (ε) are specified for all fluxes. Reactions that do not change the net number of C–C bonds, for example, isomerizations, were assumed to have values of $\varepsilon = 0$. The fractionation by PEPC (O'Leary, Rife, & Slater, 1981), which uses HCO_3^- as a substrate, was specified relative to CO_2 by adjusting for the equilibrium isotope effect ($\varepsilon_{equil\_HCO3\leftrightarrow CO2}$; Table S3). All other values of ε ($\varepsilon_{Rubisco}$; ε_{PDH}; ε_{PEPCK}; and $\varepsilon_{respiration}$) were assumed to be unknowns falling within initial boundary ranges constrained by prior literature (Table S3).

Solutions were obtained by Monte Carlo trials (n = 50,000 for autotrophic; n = 4,000 for heterotrophic) in which the unknown fluxes (*B*, *C*, *K*, φ_5) and isotope effects were resampled from broad initial ranges (Table S3). Error in the model output was determined by comparing the predicted values for each subcellular pool (e.g., FA, Asx) to the experimental values. Optimization was defined as the minimum sum of absolute values of the differences, and for each scenario (CO_2 or acetate-assimilating), the "best" solution was defined as the average of the five best trials. Because the values of ε must be the same for both culture conditions, the autotrophic scenario was run first and the best-fit isotope effects were imposed on the acetate scenario, reducing the number of trials needed to sample the variable space for the latter simulation.

3 | RESULTS AND DISCUSSION

3.1 | Photoautotrophic and photoheterotrophic bulk biomass

A stable daily optical density for *A. vinosum* DSM 180^T (Abs_{600}) of 0.52 ± 0.15 (autotrophic experiment) and 0.50 ± 0.06 (heterotrophic

TABLE 1 Summary of $\delta^{13}C$ data (‰, ±1σ) for chemostat cultures of *Allochromatium vinosum* DSM180^T

Substrate					
CO_2	−37.1				
Acetate	−46.0				
Biomass	**EA**	**SWiM**	$\varepsilon_{substrate\text{-}bio}$		
Photoautotrophy	−59.9 ± 0.1	−59.1 ± 1.9	24.3		
Photoheterotrophy	−45.9 ± 0.3	−45.8 ± 0.8	−0.1		
Proteins, nucleic acids	**All Prot.**	**Q1&2 Prot.**	**RNA**	$\varepsilon_{bio\text{-}protein}$	$\varepsilon_{bio\text{-}RNA}$
Photoautotrophy	−57.8 ± 1.8	−58.2 ± 0.9	−57.9 ± 0.3	−1.8	−2.1
Photoheterotrophy	−46.6 ± 1.2	−46.7 ± 0.7	−45.3 ± 0.5	0.8	−0.6
Lipids	**Fatty-Acids**	**Phytol**	$\varepsilon_{bio\text{-}FA}$	$\varepsilon_{bio\text{-}Phytol}$	
Photoautotrophy	−64.4 ± 0.5	−62.3 ± 2.0	4.8	2.6	
Photoheterotrophy	−46.3 ± 0.3	−51.2 ± 0.3	0.4	5.6	

experiment), pH (7.46 ± 0.06, autotrophic; 7.63 ± 0.02, heterotrophic), and E_h (−177 ± 59 mV, autotrophic only) was observed throughout the sampling periods (Fig. S1). The autotrophic condition was maintained for >2 months. The heterotrophic condition was started from fresh inoculum and maintained for 1.5 months. Under these chemostat conditions limited by phosphate, there is an excess supply of carbon substrate—either CO_2 or acetate. This enables us to compare relative variations in intracellular $\delta^{13}C$ values caused by expression of different carbon metabolic pathways, without concern that these fractionations are induced by temporal variations in carbon limitation, for example, as would be observed in batch cultures. Correspondingly, the $\delta^{13}C$ values of whole cells remained stable, −59.1 ± 1.9‰ and −45.8 ± 0.8‰, as measured daily (Fig. S1; Table 1). For each experiment, samples from multiple consecutive days were homogenized and then subdivided for the various organic chemical and isotopic analyses, smoothing out the already small day-to-day variability.

During photolithoautotrophic growth, H_2S and other reduced sulfur species serve as electron donors for CO_2 fixation using Rubisco form IA (Viale, Kobayashi, & Akazawa, 1989; Weissgerber et al., 2011). During photoorganoheterotrophic growth, the cells use acetate as both the carbon substrate and the electron donor (Weissgerber, Sylvester, et al., 2014; Weissgerber, Watanabe, et al., 2014). The measured $\delta^{13}C$ values of bulk biomass reflect the isotope fractionations associated with these processes, relative to the initial substrates. Our results show a fractionation ($\varepsilon_{substrate\text{-}bio}$; $\varepsilon = 1{,}000 \times (\alpha_{A/B} - 1)$, where $\alpha_{A/B} = (\delta_A + 1{,}000)/(\delta_B + 1{,}000)$) of 24.3‰ for CO_2 fixation, typical of other reports of microbial type IA and IB Rubisco (Guy, Fogel, & Berry, 1993; Scott et al., 2007) and consistent with an earlier study of *A. vinosum* (Quandt, Gottschalk, Ziegler, & Stichler, 1977). In contrast, $\varepsilon_{substrate\text{-}bio}$ was essentially 0‰ for acetate assimilation (Table 1). Although growing heterotrophically, this culture did not experience a "typical" bulk ^{13}C enrichment of ca. 1–1.5‰ relative to substrate, as is observed for higher heterotrophs growing on complex food sources (Deniro & Epstein, 1978).

3.2 | Fatty acids and phytols

Fatty acids were measured (as FAMEs) in lipid fractions nominally representing original glycolipids and phospholipids, although there were no significant differences observed between the two classes. Four to five major FA were identified in both experiments, with relative abundances agreeing with previous reports (Imhoff & Bias-Imhoff, 1995): $C_{18:1\omega7} > C_{16:1\omega7} > C_{16:0} > C_{18:1\omega5} \gg C_{18:0}$. The relative abundances were the same in heterotrophic and autotrophic cells, in agreement with observations of unaltered lipid composition in *A. vinosum* when grown on malate versus CO_2 (using several different sulfur species as electron donors; Weissgerber, Sylvester, et al., 2014).

Constant $\delta^{13}C$ values for all FA, −64.4 ± 0.5‰ and −46.3 ± 0.3‰ in autotrophic and heterotrophic cultures, respectively, confirm a lack of isotopic discrimination during chain-length extension or desaturation (Table 1; Fig. S2). Expressed fractionation relative to biomass ($\varepsilon_{bio\text{-}FA}$) of 4.8‰ during growth on CO_2 is typical of other bacterial and algal photoautotrophs (Sakata et al., 1997; Schouten et al., 1998), and slightly larger than *Escherichia coli* grown on glucose (~3‰; Blair et al., 1985; Monson & Hayes, 1982). Fractionation was effectively absent when acetate was the carbon source, in agreement with observations of *E. coli* grown on acetate (Deniro & Epstein, 1977).

Phytol also was ^{13}C-depleted relative to biomass in both the autotrophic and heterotrophic cultures ($\varepsilon_{bio\text{-}phytol}$ of 2.6‰ and 5.6‰, respectively). However, fractionation for phytol varied in both magnitude and direction relative to FA: Phytol was ca. 2‰ enriched in ^{13}C relative to FA in the photoautotrophic culture, but ca. 5‰ depleted in ^{13}C relative to FA in the photoheterotrophic culture (Table 1, Figure 1). The 2‰ enrichment relative to *n*-alkyl lipids in the photoautotrophic culture is consistent with other reports of CO_2-fixing organisms (Hayes, 2001; Sakata et al., 1997; Schouten et al., 1998, 2008). The only report of which we are aware that compares phytol ^{13}C patterns for photoheterotrophy versus photoautotrophy is for the related taxon, *Chromatium tepidum* (Madigan, Takigiku, Lee, Gest, & Hayes, 1989). In this organism, phytol also was more strongly ^{13}C-depleted

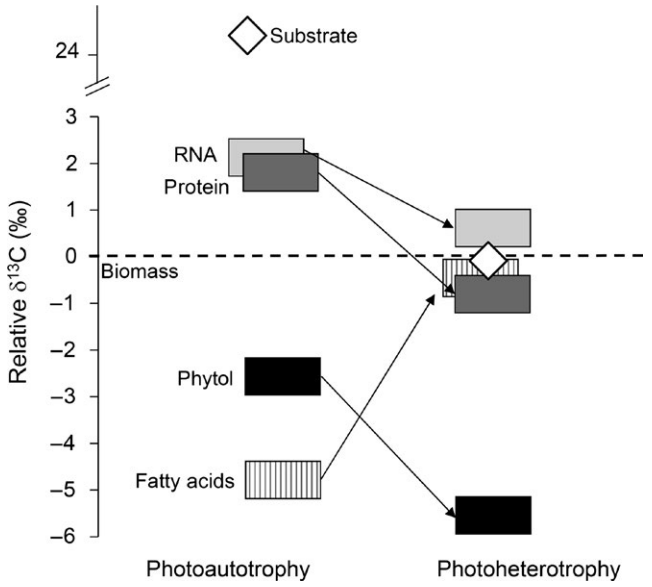

FIGURE 1 The relative distribution of $\delta^{13}C$ values for molecular classes and bulk biomass of *Allochromatium vinosum* DSM 180^T grown on CO_2 or acetate shows the reorganization of phytol and fatty acids, as well as a compressed range for biomacromolecules relative to bulk material, when cells are grown photoheterotrophically on acetate

for the acetate-grown culture than for the autotrophic culture, but *n*-alkyl lipids were not reported for comparison.

3.3 | Amino acids

Amino acid concentrations were relatively constant in both autotrophic and heterotrophic cells, with Asx, Glx, and Leu being the most abundant AAs (Table S1). Their carbon isotopes (individual $\delta^{13}C_{AA}$ values) exhibited significant intracellular variations in both the autotrophic and heterotrophic cultures (range of 20‰ among individual AAs). Such large intracellular carbon isotope variability is seen in other taxa and is presumed to be associated with the diverse metabolic pathways involved in AA synthesis (Abelson & Hoering, 1961; Larsen, Taylor, Leigh, & Brien, 2009; Macko, Fogel, Hare, & Hoering, 1987; Scott et al., 2006). Total AAs from photoautotrophy were ca. 2‰ ^{13}C-enriched relative to bulk biomass, while total AAs from photoheterotrophy were ca. 0.5‰ ^{13}C-depleted relative to bulk biomass (Figure 1). There was no significant difference between simple mean and codon-weighted approaches to averaging the net values of $\delta^{13}C_{AA}$ (Table 2), so fractionations (ε_{AA}) were calculated relative to the simple mean. Within the individual AAs, Asx, Gly, and Thr were the most ^{13}C-enriched, while Leu, Ile, and Phe were the most ^{13}C-depleted (Figure 2). These relative patterns in ^{13}C distribution generally were similar for both cultures, with the major exceptions being a ca. 6–7‰ relative enrichment for glutamate-family AAs (Glx and Pro) and a ca. 3–4‰ depletion for aspartate-family AAs (Asx, Thr, and Lys) in the acetate-assimilating culture.

3.4 | Protein and nucleic acid stable isotope ratios

Unlike the variability among individual AAs, carbon isotope values for whole proteins were fairly constant: 1.8‰ ^{13}C-enriched and 0.8‰ ^{13}C-depleted in autotrophic and heterotrophic cells, respectively (Table 1, Fig. S3). This is also in good agreement with the average AAs. Proteins from both experiments exhibit a Gaussian distribution of $\delta^{13}C$ values, and the width of this fit scales with protein concentration (which in turn determines the measurement precision; Mohr et al., 2014). The standard deviation of values (1σ) is <1‰ for the more

TABLE 2 Carbon isotope data for individual amino acids

		Photoautotrophy		Photoheterotrophy	
AA	**Family**	**$\delta^{13}C$ (‰)**	**ε_{AA} (‰)[a]**	**$\delta^{13}C$ (‰)**	**ε_{AA} (‰)[a]**
Asx	A	−47.1 ± 0.4	−10.2	−39.2 ± 0.6	−7.5
Thr	A	−49.9 ± 0.8	−7.3	−42.4 ± 0.2	−4.1
Lys	A	−50.0 ± 0.5	−7.2	−43.3 ± 0.8	−3.2
Ile	A	−65.7 ± 0.3	9.5	−53.9 ± 0.3	8.0
Gly	PGA	−49.6 ± 0.1	−7.6	−38.9 ± 0.2	−7.8
Ala	Py	−58.5 ± 0.3	1.8	−50.7 ± 0.3	4.6
Leu	Py	−65.9 ± 0.4	9.7	−53.2 ± 0.2	7.2
Glx	αKg	−58.7 ± 0.1	2.0	−41.9 ± 0.3	−4.7
Pro	αKg	−60.1 ± 0.2	3.5	−44.1 ± 0.5	−2.4
Tyr	PEP/E4P	−56.8 ± 1.1	0.0	−47.6 ± 0.8	1.3
Phe	PEP/E4P	−62.9 ± 0.5	6.5	−54.8 ± 0.2	8.9
Mean $\delta^{13}C_{AA}$		**−56.8 ± 0.4**		**−46.4 ± 0.4**	
$\delta^{13}C_{proteome}$, codon-weighted[b]		**−57.1**		**−46.2**	

[a]$\varepsilon_{AA} = 1{,}000((\delta_{mean} + 1{,}000)/(\delta_{AA} + 1{,}000) - 1)$.
[b]Codon-weighted mean values calculated in proportion to genome-wide codon usage (http://www.kazusa.or.jp/codon/cgi-bin/showcodon.cgi?species=1049).

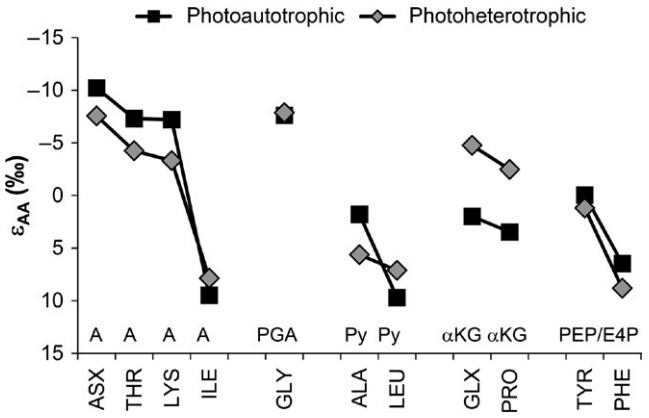

FIGURE 2 Individual amino acids from photoautotrophic and photoheterotrophic cultures grouped by biosynthetic category as defined in Hayes (2001). ε_{AA} is calculated as the fractionation relative to the mean for all measured AAs. By convention, positive values of ε imply discrimination against ^{13}C (i.e., Ile is the most ^{13}C-depleted AA); the *y*-axis is inverted to the intuitive direction

abundant proteins but larger for the low-concentration proteins, suggesting that σ is a measure of aggregated analytical errors, rather than actual intracellular variability. Similar results were observed for the cyanobacterium *Synechocystis* sp. PCC 6803 (Mohr et al., 2014). The relative agreement between average $\delta^{13}C_{protein}$, $\delta^{13}C_{AA}$, and $\delta^{13}C_{biomass}$ values is expected, as protein accounts for the quantitative majority of cell carbon. It is not necessarily a given, however, that within these averages, $\delta^{13}C$ values of *individual proteins* would have a narrow range. Although proteins reflect mass-weighted mixtures of the AAs, differences in timing of synthesis, resource allocation, and various post-translational modifications (PTM; Weissgerber, Sylvester, et al., 2014; Weissgerber et al., 2011) could induce isotopic variability. Our results show that these metabolic variations and carbon added by PTM have little impact on $\delta^{13}C$ signatures of individual proteins within the cell.

Values of $\delta^{13}C$ for extracted nucleic acids were similar to observations for proteins, with $\varepsilon_{bio\text{-}RNA}$ of −2.1‰ and −0.6‰ in autotrophic and heterotrophic cells, respectively (Table 1, Figure 1).

3.5 | Proteomics

Enzymes of key biosynthetic pathways had different abundances between the two cultures. Similar to a recent proteomic study of *A. vinosum* DSM 180^T grown autotrophically and on malate (Weissgerber, Sylvester, et al., 2014), differences were observed for both carbon-assimilating and energy-metabolism enzymes (Figures 3, 4, Table S2). Differences in protein expression between the two conditions were compared using cluster diagrams (largest relative differences per KEGG category; Figure 3). These differences were mapped onto a metabolic pathway diagram (Figure 4) to highlight the enzymes that showed the greatest relative changes within the carbon-fixing and central metabolic pathway modules.

Examples of relatively increased enzyme concentrations in the acetate-assimilating culture include higher levels of dethiobiotin synthase and 3-oxoacyl-ACP synthase. The first makes biotin, an essential cofactor for carboxylation reactions such as conversion of acetyl-CoA to malonyl-CoA; while the second participates in acetyl chain elongation, a step for building the C_2 acetate substrate into larger metabolites. The acetate-assimilating culture also contained relatively higher quantities of enzymes involved in polysaccharide cycling, for example, glycogen phosphorylase, possibly to increase cellular storage products during conditions of repressed CO_2-fixation. Examples of increased abundance for the autotrophic culture include glyceraldehyde-3-phosphate dehydrogenase and transketolase, both necessary for the production of simple sugars as the primary metabolites in CO_2-fixation by the CBB cycle. The greatest relative change in expression, however, was ME (discussed below). Finally, *A. vinosum* also contains two sets of Rubisco genes (Viale et al., 1989). Our protein results indicate *rbcAB* is expressed more strongly in the CO_2 culture and *rbcSL* more strongly in the acetate culture. The latter is associated with carboxysome genes and is expressed preferentially at low CO_2 concentrations (Badger & Bek, 2008; Weissgerber et al., 2011). Preferential expression of *rbcAB* during autotrophy also was observed by Weissgerber, Sylvester, et al. (2014), but they were unable to detect the products of *rbcSL* during growth on malate, while here we were able to detect low-level *rbcSL* expression during growth on acetate. Measurable Rubisco in the heterotrophic culture is consistent with its use in recycling intracellular CO_2 or for CO_2 fixation at the low background concentration of the growth medium.

3.6 | Isotope flux-balance model

The isotopic patterns observed in the two cultures can be understood as resulting directly from the route of carbon entry into metabolic pathways, in combination with the isotope effects expressed in the formation of central intermediates. To examine the resulting fractionation, we constructed a steady-state, isotope flux-balance model following the branched reaction network approach of Hayes (2001). The model takes a simplified approach to central metabolism and can simulate acetate assimilation or CO_2 fixation by changing the input fluxes (φ_1 = acetate; φ_2 = CO_2; Tables 3, S4, Fig. S4).

The model was solved for the relative carbon fluxes in photoautotrophic versus photoheterotrophic *A. vinosum* as well as the $\delta^{13}C$ values for the resulting biomass pools (Table 3, Figure 5). The predicted fraction of initial carbon flux (φ_1 or $\varphi_2 \equiv 1$) assimilated to biomass, *B*, is 0.69 for autotrophy and 0.87 for photoheterotrophic acetate assimilation. Total carbon input to the cell, however, includes both this initial flux and the significant additional carbon derived from anaplerotic carbon fixation (PEPC and/or PEPCK). Accounting for this extra carbon in the photoautotrophic scenario results in a net *B* yield of 0.53, and an anaplerotic flux equal to 22% of the total carbon input. The corresponding budget for the acetate-assimilating scenario is 29% of cell carbon incorporated by anaplerotic reactions, and a net *B* yield of 0.61. These values of *B* are within the range reported for a similar metabolic flux study on *Synechocystis* sp. PCC6803 (Yang, Hua, & Shimizu, 2002). The estimates of anaplerotic carbon fixation are higher than previously reported for photoheterotrophic bacteria (Tang, Feng, Tang, & Blankenship, 2009), although

TABLE 3 Optimized results of isotope flux-balance model; see also Tables S3, S4, and Fig. S4

Biomass yield[a]	Relative fraction			
φ_{30}; *n*-Alkyl lipids (fatty acids)	0.15			
φ_{28}; Isoprenoid lipids	0.01			
φ_{27}; Ala; Leu+ (Ala; Leu, Val)	0.14			
φ_{24}; Gly+ (Gly, Ser, Cys, Tyr, Trp, Phe; sugars of NA)	0.27			
φ_{25}; Asx; Thr+ (Asx; Thr, Lys, Ile, Met; 50% of NA bases)	0.22			
φ_{26}; Glx; Pro+ (Glx; Pro, Arg, His; 50% of NA bases)	0.21			
Isotope effects[b]	ε (‰)			
$\varepsilon_{Rubisco}$	27			
ε_{PEPCK}; ε_{PS}	25			
ε_{PEPC}	−7[c]			
$\varepsilon_{respiratory}$	0			
ε_{PDH}	8.5[d]			
Flux assumptions	**Autotrophic**		**Heterotrophic**	
φ_1; Acetate uptake	0		1	
φ_2; CO_2 uptake	1		0	
$\varphi_{3,17}$; AcCoA carboxylase	0		>0	
$\varphi_{4,18}$; Pyruvate dehydrogenase	>0		0	
	Autotrophic		**Heterotrophic**	
Solutions	**Tested**	**Optimal**	**Tested**	**Optimal**
Tunable parameters				
B; Fraction of carbon input → biomass	0.3 to 0.7	0.69	0.6 to 0.9	0.87
C; Isocitrate lyase branch point ($\varphi_{14}/(\varphi_8 + \varphi_9)$)	0.0 to 0.3	0.12	0.05 to 0.2	0.097
K; Relative PEPCK versus PEPC (φ_7/φ_6)	−0.4 to 0.3	−0.38	−0.8 to 0.8	−0.36
φ_5; PEP ↔ pyruvate	0.2 to 0.8	0.27	−1.4 to 0.2	−0.71
Fluxes				
$\varphi_{3,17}$; Pyruvate synthase (PS)		0		0.35
$\varphi_{4,18}$; Pyruvate dehydrogenase (PDH)		0.38		0
$\varphi_{6,19}$; PEPC (HCO_3^-)		0.87		0.75
$\varphi_{7,20}$; PEPCK (CO_2)		−0.33		−0.27
$\varphi_{8,9}$; Citrate synthase, aconitase		0.71		1.36
φ_{10}; Isocitrate dehydrogenase		0.48		0.97
$\varphi_{11,22}$; 2-oxoglutarate dehydrogenase		0.27		0.63
φ_{12}; Malate oxidoreductase		−0.098		0.46
$\varphi_{13,23}$; Malate dehydrogenase (malic enzyme)		0.41		0.32
$\varphi_{14,15}$; Isocitrate lyase		0.13		0.20
φ_{16}; Malate synthase		0.088		0.13
$\varphi_{28,29}$; Deoxyxylulose-5-phosphate synthase		0.007		0.009

[a]Determined from measured AA abundances (this work) and metabolite abundances (Weissgerber, Watanabe, et al., 2014).
[b]Consensus values from Monte Carlo trials based on literature ranges (e.g., Hayes, 2001); see Table S3.
[c]$\varepsilon = \varepsilon_{PEPC} - (\varepsilon_{equi\_HCO3 \leftrightarrow CO2}) = 2‰ - (9‰) = -7‰$, approximated at 25°C; PEPC from O'Leary et al., 1981.
[d]Net ε for production of acetate from pyruvate (7–12‰) is half the position-specific fractionation (15–23‰; Deniro & Epstein, 1977; Melzer & Schmidt, 1987; Monson & Hayes, 1982); consensus from model trials is 8.5‰.

Yang et al. (2002) reported that PEPC accounted for 25% of assimilated carbon in *Synechocystis* grown mixotrophically and on glucose. Similarly, anaplerotic contributions in eukaryotic algae generally are assumed to average ~10% of carbon fixation, but wider ranges (up to 27%) have been reported under some growth conditions (Cassar & Laws, 2007). In both model solutions for *A. vinosum*, the large anaplerotic flux is attributed entirely to the activity of PEPC, and PEPCK is predicted to operate only in the decarboxylation direction. This

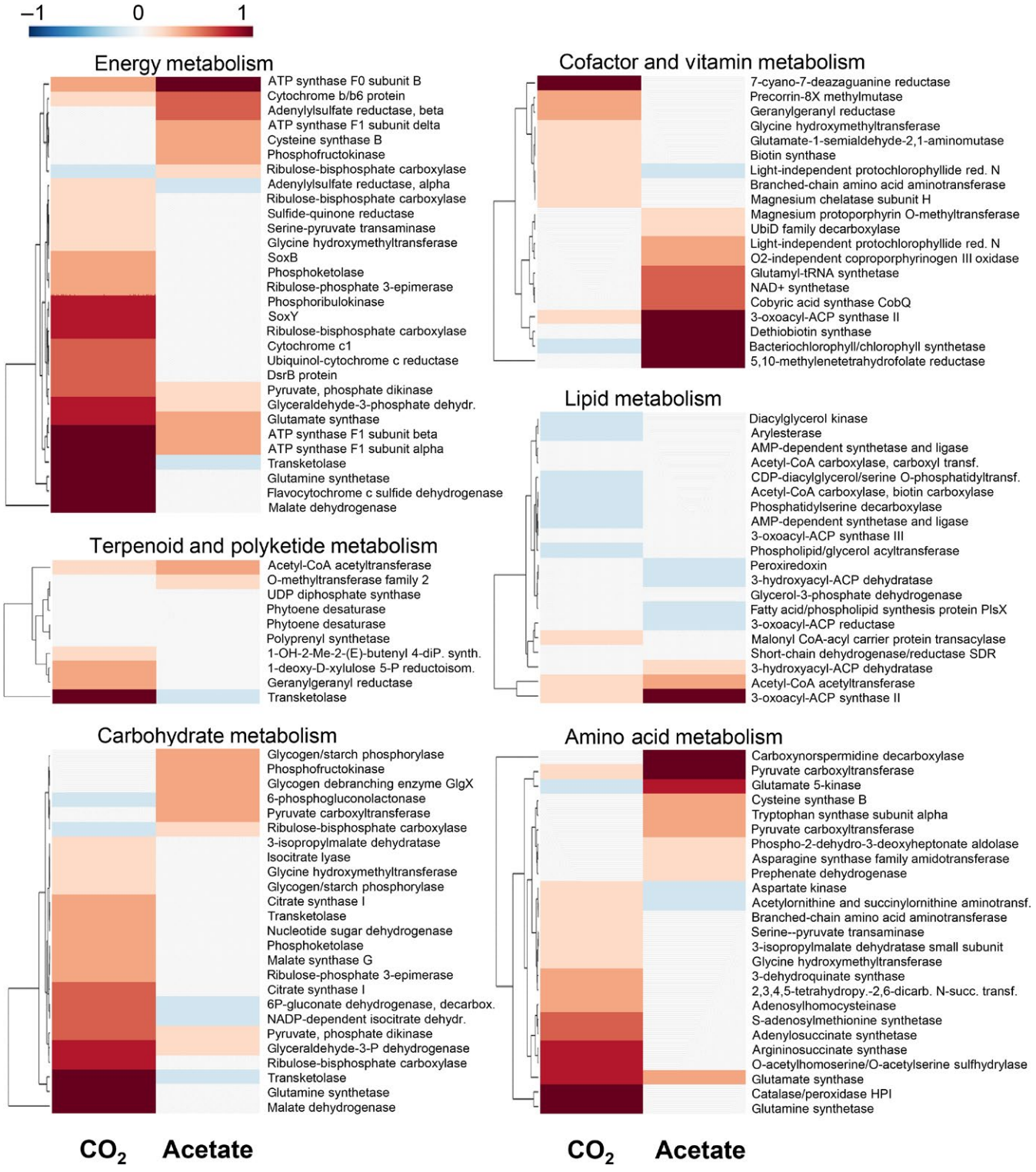

FIGURE 3 Cluster diagrams showing proteins with the largest differences in relative detection between the two experiments, as grouped by KEGG orthology. Differences are calculated as the difference between *z*-scored abundance, rather than absolute abundance, to normalize the two experiments to a uniform scale. Enzyme names, EC numbers, and scores, Table S2

is consistent with the interpretation generally applied to PEPCK in higher plants (including C_4 plants) (Chen, Walker, Acheson, & Leegood, 2002; Leegood & Walker, 2003; Urbina & Avilan, 1989), although the enzyme is believed to operate reversibly in marine algae (Raven & Beardall, 2015).

3.6.1 | The importance of malic enzyme

In agreement with a large anaplerotic flux, in both cases the model predicts the majority of oxaloacetate (OAA) is produced by PEPC-mediated carboxylation of PEP, rather than from cyclic return flow

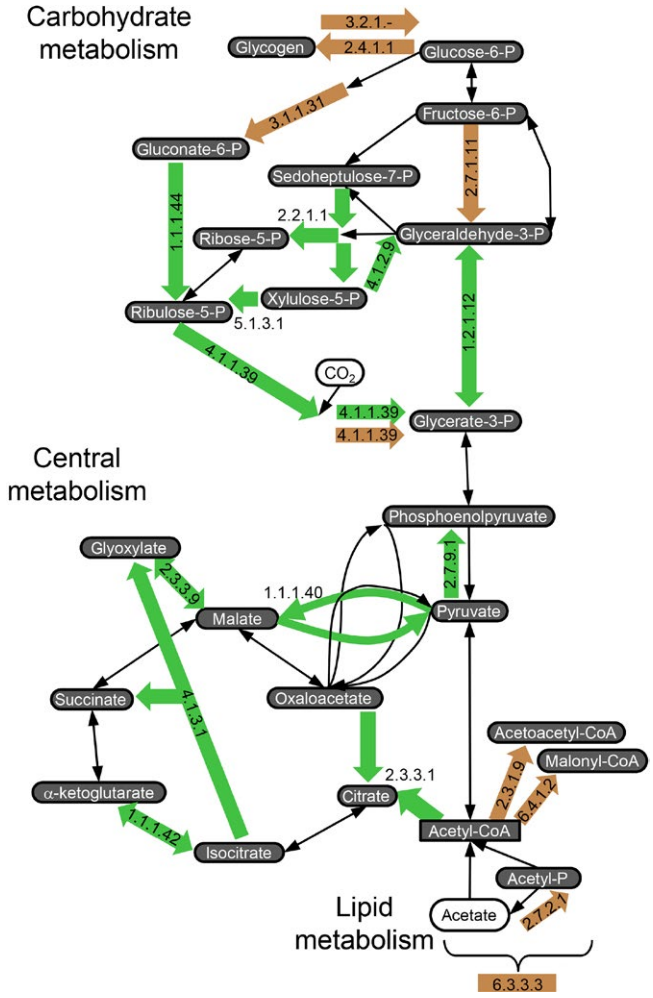

FIGURE 4 Condensed metabolic map showing differences between *Allochromatium vinosum* DSM 180^T grown on CO_2 (green) or acetate (brown). The enzymes highlighted with colored arrows are those from Figure 3, with the color specifying in which experiment the activity was enhanced. Some intermediate pathway steps are omitted for simplicity. Enzyme names, EC numbers, and scores, Table S2

through the TCA cycle. In CO_2-fixing *A. vinosum*, all malate appears to exit the TCA cycle by decarboxylation to pyruvate, where it is then further decarboxylated to acetyl-CoA and finally reincorporated with OAA into citrate. OAA in the photoheterotrophic scenario instead derives both from PEP and from cyclic return of malate → OAA in the TCA cycle. The malate → pyruvate (ME) exit route is somewhat diminished in this scenario, although still significant. Associated with these differences, the largest relative change in protein expression between the two experiments is the enhancement of ME (E.C. 1.1.1.40) during photoautotrophy (Figures 3 and 4).

This finding suggests a different interpretation of the results of Weissgerber, Sylvester, et al. (2014) and Weissgerber, Watanabe, et al. (2014), who also found evidence for an important role for ME during both heterotrophic growth on malate and autotrophic growth on CO_2. They suggested that ME is under reversible control in *A. vinosum*: decarboxylating when malate is the primary carbon substrate, but carboxylating during autotrophy, that is, performing anaplerotic replenishment of TCA cycle intermediates. Instead, our model indicates that the function of ME during autotrophic growth is decarboxylation. This may be a common feature in bacterial photoautotrophy, as the cyanobacterium *Synechocystis* sp. PCC6803 gave similar results (Bricker et al., 2004; Yang et al., 2002; Young, Shastri, Stephanopoulos, & Morgan, 2011). Malic enzyme may be a critical gatekeeper that promotes extensive carbon fixation into the C_4 intermediate, OAA, by limiting the amount of OAA that returns via the TCA cycle. Moreover, as *A. vinosum* has a complete TCA cycle—unlike *Synechocystis* and other cyanobacteria (Tang, Tang, & Blankenship, 2011)—the enhanced PEPC and ME activity in this taxon cannot be due to the need to compensate for TCA cycle deficiencies. Rather, it suggests that this mechanism, which has biochemical similarity to the C_4 pathway of plants and diatoms (Reinfelder, 2011), may be broadly distributed among photosynthetic bacterial taxa to promote the formation of C_4 acids.

3.6.2 | Controls on the ^{13}C distribution of lipids

The model, despite its relative simplification of cellular metabolic networks, can adequately explain the patterns of $\delta^{13}C$ values observed for the cellular biomass components (Figure 5). Errors for the FA and isoprenoid predictions are within 0.6‰ of observations in the photoautotrophic scenario and within 0.3‰ in the photoheterotrophic scenario; that is, the model easily generates the isotopic inversion of phytol relative to FAs. The model also confirms that the ^{13}C-enriched character of Asx for both experiments (error of −0.9‰ for the autotrophic model; error of 0.0‰ for the photoheterotrophic model) is due to the large flux from PEP → OAA by PEPC, which is specific for HCO_3^-.

Acetogenic lipids have $\delta^{13}C$ signatures that reflect acetyl-CoA (ACC), which during growth on acetate is derived directly from substrate assimilation. Further polymerization of ACC to FA is not accompanied by significant fractionation, that is, $\varepsilon_{bio\text{-}FA}$ = 0‰, consistent with earlier observations (Deniro & Epstein, 1977; Figure 6a). In contrast, FA are depleted in ^{13}C relative to pyruvate (PYR) in the CO_2-fixing experiment due to fractionation during the decarboxylation of pyruvate by pyruvate dehydrogenase (PDH). The observed value of $\varepsilon_{bio\text{-}FA}$ is ca. 5‰, while the model prediction is closer to 6‰ (Figure 6b). The magnitude of this fractionation is controlled by the critical branch point between the path PEP → PYR → ACC (φ = 0.38) versus the path PEP → OAA (φ = 0.87). This is equivalent to directing 30% of the carbon to ACC. Because the isotope effect is expressed specifically at the C-2 position of pyruvate (Monson & Hayes, 1982), $\varepsilon_{C\text{-}2}$ is 17‰, or twice that presumed for net reaction of PDH (ε_{PDH} = 8.5‰). The 5–6‰ $\varepsilon_{bio\text{-}FA}$ fractionation for the synthesis of FA by autotrophic *A. vinosum* is twice as large as the ca. 3‰ $\varepsilon_{bio\text{-}FA}$ values reported for studies of *E. coli* growing on glucose (Blair et al., 1985; Monson & Hayes, 1982), despite the similar value of $\varepsilon_{C\text{-}2}$ = 21‰ for *E. coli* PDH (Melzer & Schmidt, 1987). Highly fractionated FA are direct evidence for a relatively small flux in the direction of PEP → PYR → ACC ($f_{PYR \rightarrow ACC}$; Figure 6b). If this finding

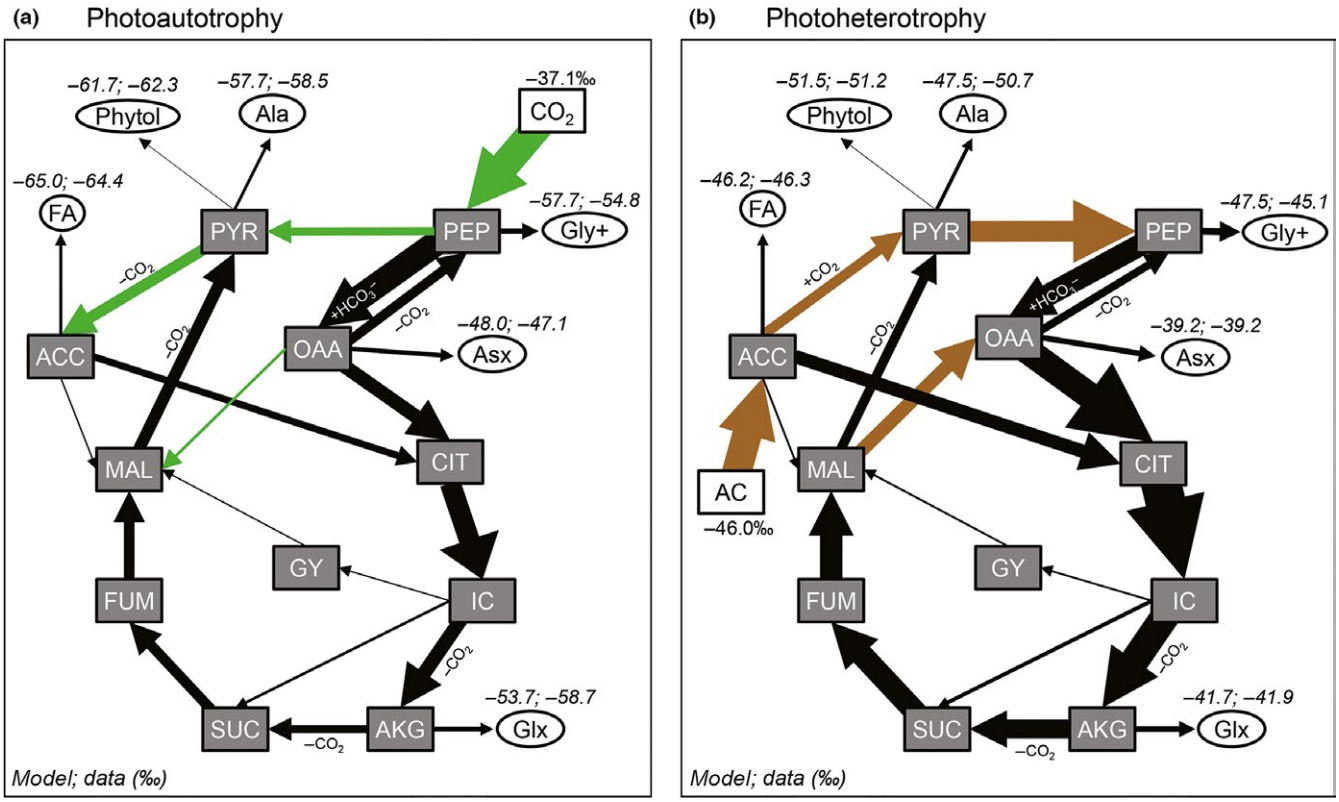

FIGURE 5 Results of the isotope flux-balance model calculated for phototrophic growth of *Allochromatium vinosum* DSM 180^T on (a) CO_2 and (b) acetate. Colored arrows show fluxes that are predicted to change direction between the two scenarios; widths of all arrows are proportional to the predicted fluxes. Isotope results are shown in the order: model, experimental data. Abbreviations: FA, fatty acids, *n*-alkyl lipids; ISP, isoprenoid lipids; ALA, alanine; GLY+, glycine-family amino acids; ASX, aspartate-family amino acids; GLX, glutamate-family amino acids; AC, acetate; ACC, acetyl-CoA; PYR, pyruvate; PEP, phosphoenolpyruvate; OAA, oxaloacetate; CIT, citrate; IC, isocitrate; AKG, 2-oxoglutarate; SUC, succinate; FUM, fumarate; MAL, malate; GY, glyoxylate. Full model topology and parameters are shown in Fig. S4, Tables S3, and S4.

can be generalized to other photoautotrophic bacteria, the extent of ^{13}C-depletion in FAs relative to biomass may be an indicator of the importance of PEPC activity (C_4 acid production). Similarly, in experiments with *Synechocystis* sp. UTEX 2470, the FA were ^{13}C-depleted relative to biomass by an average of 9‰, leading the authors to conclude that only 22% of the carbon entering the PEP + PYR pool was decarboxylated to ACC (Sakata et al., 1997), even less than for *A. vinosum*.

Other phototrophic microbial communities and environmental isolates are consistent with these interpretations. Microbial mats and microbialites in lakes show values of $\varepsilon_{bio\text{-}FA}$ between 5‰ and 7‰ (Brady, Druschel, Leoni, Lim, & Slater, 2013; Brady et al., 2010), while stromatolites from Shark Bay, Australia, also have values of $\varepsilon_{bio\text{-}FA}$ ca. 7‰ (Pagés et al., 2014). *Phormidium* isolates from Yellowstone National Park mats show larger $\varepsilon_{bio\text{-}FA}$ values (ca. 10‰, Jahnke et al., 2004), similar to the fractionation observed by Sakata et al. (1997). Together, the data point to greater fractionation in the synthesis of FA by microbial photoautotrophs relative to heterotrophic bacteria, with the greatest fractionation occurring among cyanobacteria (Blair et al., 1985; Monson & Hayes, 1982; Teece, Fogel, Dollhopf, & Nealson, 1999). This may be understood—somewhat counterintuitively—as the result of the relatively high flux of PEP through C_4 carbon fixation during photoautotrophy.

Isoprenoid lipids in photoautotrophs generally are ^{13}C-enriched relative to FA (Hayes, 2001). Most bacteria—including *A. vinosum*, other sulfur-oxidizing phototrophs, and cyanobacteria—synthesize isoprenoids from PYR and glyceraldehyde-3-phosphate (G3P), forming 2-C-methylerythritol-4-phosphate (MEP; Lichtenthaler, Rohmer, & Schwender, 1997; Rohmer et al., 1993). Our model generates MEP-pathway isoprenoids solely from pyruvate, because although G3P is more closely related to PEP, the model treats PYR and PEP as isotopically equivalent. We then apply an empirical fractionation of $\varepsilon_{isoprenoid}$ = 4‰ associated with synthesis of MEP, to achieve best fit with the autotrophic phytol data (Figure 5). The magnitude of this number may be associated with the condensation of PYR and G3P, or with the subsequent decarboxylation of MEP. Formulated in this way, the model can predict the sensitivity of $\delta^{13}C_{Phytol}$ values to changes in metabolite flux. For example, if the fraction of carbon flowing to ACC decreases, the δ^{13}C values of both Ala and phytol should decrease in parallel with the isotopic composition of FA (Figure 6b). Alternatively, if $f_{PYR\rightarrow ACC}$ approaches 0.5, the value of $\delta^{13}C_{Phytol}$ should approach $\delta^{13}C_{biomass}$.

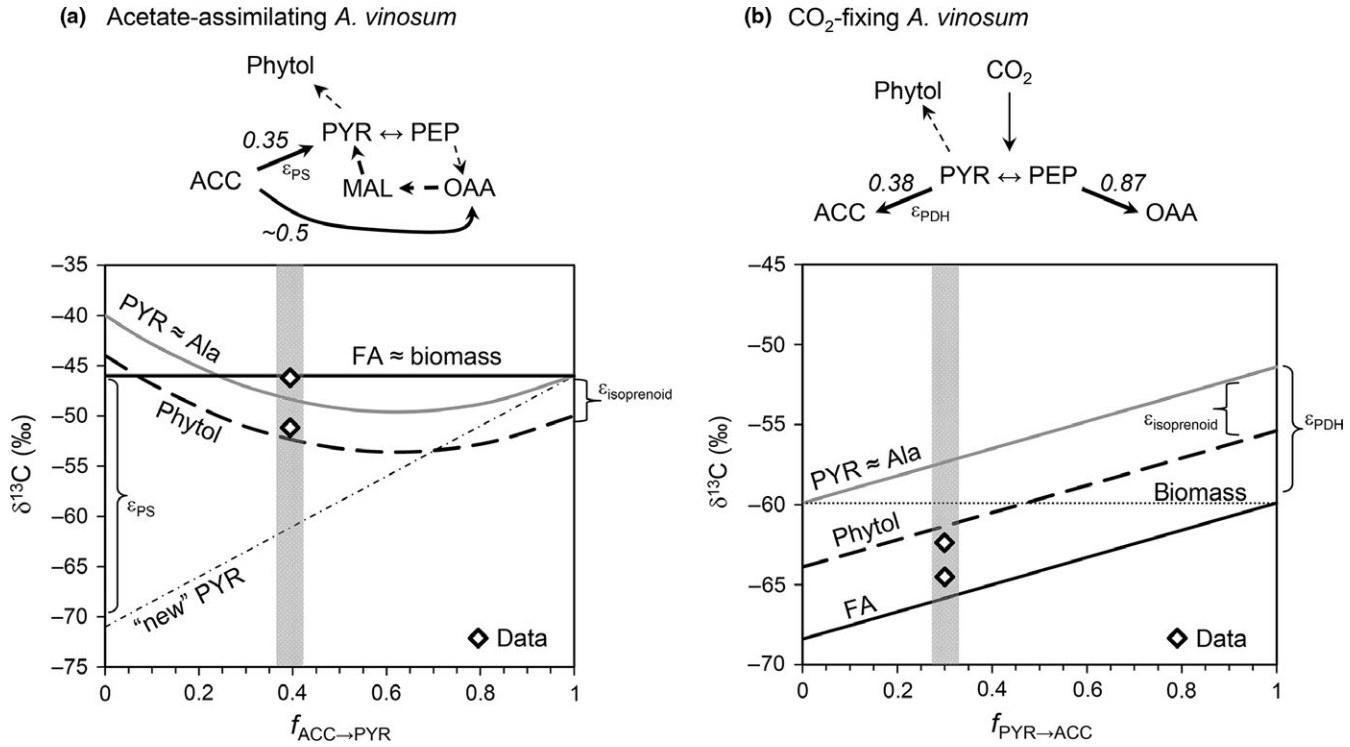

FIGURE 6 Diagrams summarizing the modeled flows of carbon that influence lipid ^{13}C distributions in *Allochromatium vinosum*. (a) During acetate assimilation, FA and biomass are isotopically identical. PYR, the precursor to phytol and Ala, contains contributions both from the activity of pyruvate synthase (PS) and from the flow from MAL → PYR. "New PYR" is ^{13}C-depleted, but it is counterbalanced isotopically by MAL, such that total PYR, Ala, and phytol are predicted to have low sensitivity to changes in metabolic flow ratios over the entire mid-range of $f_{ACC\rightarrow PYR}$. This implies that phytol should be consistently ^{13}C-poor relative to biomass in acetate-assimilating taxa. The data and model agree within 0.3‰ for both lipid classes. (b) During CO_2-fixation, carbon flow is split between decarboxylation of PYR to ACC (by PDH) and carboxylation of PEP to OAA (by PEPC). In this metabolic mode, PYR, Ala, phytol, and FA all are expected to respond in parallel to changes in the relative flow of carbon through this branch point. The data and model are offset by 0.6‰ in opposing directions for the two lipid classes, indicating the model does not completely capture all processes affecting ^{13}C distributions

The acetate-assimilating, photoheterotrophic scenario is not similarly sensitive. Isoprenoids and Ala-family AAs are the most ^{13}C-depleted constituents of the cell during growth on acetate (Tables 1 and 2). As PYR is immediately downstream of ACC in this scenario (via PS, ε_{PS} = 25‰), its isotopic composition will reflect a balance between the ^{13}C-depleted flux from ACC and the ^{13}C-enriched flux from malate (similar to Asx and Glx). A relatively larger respiratory demand would increase the flow from ACC → CIT, decreasing the fraction from ACC → PYR ($f_{ACC\rightarrow PYR}$) and yielding more strongly ^{13}C-depleted "new PYR" (Figure 6a). The effect of this change on the net $\delta^{13}C$ value of PYR, however, is minimal, because it is offset by an increased relative flux from malate. This implies that during acetate assimilation, PYR, Ala, and isoprenoids are all relatively insensitive to changes in $f_{ACC\rightarrow PYR}$, and they should be ca. 4–7‰ ^{13}C-depleted relative to biomass assuming $f_{ACC\rightarrow PYR} > 0.25$ (Figure 6a).

These results may provide some insight to prior observations. In CO_2-fixing *C. tepidum*, phytol was ^{13}C-depleted relative to biomass by ca. 3‰ (Madigan et al., 1989). This is virtually identical to our result for *A. vinosum* and suggests such a value may be typical for *Chromatiaceae*. However, the CO_2-fixing cyanobacteria that have greater ^{13}C-depletion in their FA—e.g., the *Phormidium* isolates from Yellowstone National Park—also have more ^{13}C-depleted phytol (ca. 4–6‰ ^{13}C-depleted relative to biomass; Jahnke et al., 2004). Similar relative fractionation was observed for phytol from *Synechocystis* UTEX 2470 (Sakata et al., 1997). These observations agree with the idea that FA and phytol in photoautotrophs should change in tandem because their respective metabolic precursors PYR and ACC should isotopically covary (Figure 6a). Strongly ^{13}C-depleted phytol and *n*-alkyl lipids relative to sedimentary organic matter may be an indicator of significant cyanobacterial input. In contrast, while acetate-assimilating photoheterotrophs also would be a source of ^{13}C-depleted phytol, the *n*-alkyl lipids from these organisms would be isotopically similar to bulk carbon.

Other discussions of the relative ^{13}C patterns between isoprenoids and biomass have focused largely on eukaryotic algae (e.g., Schouten et al., 1998, 2008). Although more complicated to interpret than bacteria, some of the same principles may apply. In particular, despite the variability in absolute values of $\varepsilon_{bio\text{-}FA}$ and $\varepsilon_{bio\text{-}Phytol}$ for various algal taxa, the *difference* between MEP-pathway phytol and plastidic FAs is a remarkably constant 3 ± 1‰ (Hayes, 2001); this generalizes to ca. 2–3‰ and 5–6‰ ^{13}C-depletion relative to biomass for phytol and *n*-alkyl lipids, respectively, similar to the CO_2-fixing *Chromatiaceae* but less fractionating than the cyanobacteria.

Finally, these predictions apply only to isoprenoids made by the MEP pathway. The classical mevalonate (MVA) pathway of eukaryotes

(Bloch, Chaykin, Phillips, & Dewaard, 1959) yields isoprenoids from acetate and would be affected—especially in photoautotrophy—by the isotope balance around ACC. The MVA pathway is rare in bacteria, occurring in some Firmicutes, Actinobacteria, and a few, often by horizontal gene transfer (Boucher & Doolittle, 2000; Lombard & Moreira, 2011), so would not be expected to quantitatively affect the sedimentary record of preserved bacterial lipids.

3.7 | Implications for interpreting the geologic record

Our results highlight the importance of understanding intracellular carbon isotope patterns when interpreting both the molecular level and bulk geochemical record of carbon preservation. The data for *A. vinosum*, when viewed in the context of other microbial photoautotrophic studies, help decipher the mechanisms underpinning lipid isotope signatures in the sedimentary record, as well as the patterns of these lipids show relative to the associated kerogen. Specifically, these signatures may reflect the importance of metabolic flexibility in how micro-organisms assimilate carbon in response to local environmental conditions. The new framework may thus help to illuminate the sources of organic matter buried in the geologic record.

The isotopic offsets for phytol and FA relative to biomass in the CO_2-fixing *A. vinosum* culture are similar to the Phanerozoic average values of 2–3‰ and 4–5‰ more negative than kerogen for pristane/phytane and *n*-alkyl lipids, respectively (Hayes, 2001; Logan et al., 1995, 1997). These offsets are typical of most Phanerozoic rocks, with some notable exceptions (e.g., Grice et al., 2005). As such, the *A. vinosum* data are broadly similar to marine algal production, both at the bulk and molecular level (Hayes, 2001; Schouten et al., 1998), and this isotopic pattern may be typical of CBB-pathway photoautotrophy in both anoxygenic phototrophs and eukaryotes. In contrast, larger ^{13}C depletions in both pristane/phytane and *n*-alkyl lipids relative to biomass (e.g., Jahnke et al., 2004) may be diagnostic for systems dominated by cyanobacterial CO_2 fixation. The larger relative fractionation may be attributed to a hypothesized greater flux through PEP carboxylase.

The interpretive challenge therefore is the mixed situation: If *n*-alkyl lipids are relatively ^{13}C-enriched in the presence of ^{13}C-poor pristane/phytane, then the explanation may be the enhanced assimilation of acetate throughout the microbial community—including by cyanobacteria, by anoxygenic phototrophs including sulfur oxidizers, and/or by heterotrophs. Isotopic reversal of *n*-alkyl lipids and pristane/phytane in the geologic record may thus be a biosignature for enhanced preservation of the products of (photo)heterotrophic carbon cycling, if such a cycle can generate significant acetate. However, by definition, net heterotrophy cannot exceed photoautotrophy. Therefore, to preserve "inverse" isotopic patterns in the geologic record, there also must be (i) at least some expression of the Logan et al. (1995, 1997) effect and/or (ii) widespread preservational biases, caused by local diagenetic effects and/or by shifts in overall facies preservation in the rock record.

Complex modes of carbon and energy cycling in microbial mats may influence the isotopic characteristics of organic carbon preserved in benthic ecosystems. Idea (ii) may be consistent with a sedimentary record that contains a disproportionate amount of benthic mat-derived carbon in which phototrophy and fermentation are major co-occurring processes. A possible modern analog for such a scenario is the microbial mat ecosystem from Middle Island Sinkhole, Lake Huron (Voorhies et al., 2012). In that environment, benthic sulfide flux supports a persistently low-O_2 community dominated by *Phormidium* spp., which overlay layers of sulfur-oxidizing chemosynthetic bacteria and sulfate reducers. Net primary production by the *Phormidium* mat is not oxygenic, but rather may switch between sulfide oxidation and O_2 production depending on sulfide availability. The mat is believed to store excess photosynthetic carbon reserves in order to ferment them to acetate at night, as has been hypothesized for phototrophic mats in other contexts (Nold & Ward, 1996). This may then permit assimilation of the resulting acetate by the other members of the bacterial community.

If such systems are similar to Proterozoic microbial mats, carbon produced by these processes may then be preferentially sequestered according to the recently proposed "mat seal" hypothesis (Pawlowska, Butterfield, & Brocks, 2012). In this hypothesis, ^{13}C-enrichment of *n*-alkanes is proposed to result from heterotrophic reworking, following the Logan et al. (1995) interpretation. Instead, here we would argue that such isotopic enrichment would also be at least in part a primary biosynthetic signal due to assimilation of acetate, and burial and long-term preservation of the lipid products of these pathways would be enhanced. To test these ideas, more work is needed to investigate other modern analog systems, as well as to examine more complex fermentative pathways (e.g., lactate fermentation; Teece et al., 1999) that may exert different influences on intracellular isotopic patterns. Regardless, our observations for the metabolically flexible, anoxygenic phototroph *A. vinosum* indicate that microbial taxa that live at redox boundary zones may switch their patterns of lipid $\delta^{13}C$ values in response to different metabolic modes of carbon incorporation, and these patterns could persist if microbial mats are preferentially preserved in the geologic record.

ACKNOWLEDGMENTS

We thank S.J. Carter for laboratory support, K.B. Herren and E.B. Wilkes for computational assistance, H. Close for advice on amino acid analysis, W. Leavitt for chemostat advice, and Jochen Brocks and three anonymous reviewers for their editorial work and valuable feedback. This work was supported by grants from the Gordon and Betty Moore Foundation (to A.P.), the NSF-DEB Dimensions of Biodiversity Program (to A.P. and P.R.G.), and by a Marie Curie International Outgoing Fellowship (to W.M.). This study is dedicated to the memory of microbial ecologist Diana Nemergut (1974–2015).

REFERENCES

Abelson, P. H., & Hoering, T. C. (1961). Carbon isotope fractionation in formation of amino acids by photosynthetic organisms. *Proceedings of the National Academy of Sciences of the United States of America*, *47*, 623–632.

Badger, M. R., & Bek, E. J. (2008). Multiple Rubisco forms in proteobacteria: Their functional significance in relation to CO_2 acquisition by the CBB cycle. *Journal of Experimental Botany*, *59*, 1525–1541.

Blair, N., Leu, A., Munoz, E., Olsen, J., Kwong, E., & DesMarais, D. (1985). Carbon isotopic fractionation in heterotrophic microbial metabolism. *Applied and Environmental Microbiology*, *50*, 996–1001.

Bligh, E. G., & Dyer, W. J. (1959). A rapid method of total lipid extraction and purification. *Canadian Journal of Biochemistry and Physiology*, *37*, 911–917.

Bloch, K., Chaykin, S., Phillips, A. H., & Dewaard, A. (1959). Mevalonic acid pyrophosphate and isopentenylpyrophosphate. *Journal of Biological Chemistry*, *234*, 2595–2604.

Boucher, Y., & Doolittle, W. F. (2000). The role of lateral gene transfer in the evolution of isoprenoid biosynthesis pathways. *Molecular Microbiology*, *37*, 703–716.

Brady, A. L., Druschel, G., Leoni, L., Lim, D. S. S., & Slater, G. F. (2013). Isotopic biosignatures in carbonate-rich, cyanobacteria-dominated microbial mats of the Cariboo Plateau, B.C. *Geobiology*, *11*, 437–456.

Brady, A. L., Slater, G. F., Omelon, C. R., Southam, G., Druschel, G., Andersen, D. T., & Lim, D. S. S. (2010). Photosynthetic isotope biosignatures in laminated micro-stromatolitic and non-laminated nodules associated with modern, freshwater microbialites in Pavilion Lake, B.C. *Chemical Geology*, *274*, 56–67.

Bricker, T. M., Zhang, S., Laborde, S. M., Mayer III, P. R., Frankel, L. K., & Moroney, J. V. (2004). The malic enzyme is required for optimal photoautotrophic growth of *Synechocystis* sp. Strain PCC6803 under continuous light but not under a diurnal light regimen. *Journal of Bacteriology*, *186*, 8144–8148.

Brocks, J. J., Love, G. D., Summons, R. E., Knoll, A. H., Logan, G. A., & Bowden, S. A. (2005). Biomarker evidence for green and purple sulphur bacteria in a stratified Palaeoproterozoic sea. *Nature*, *437*, 866–870.

Bryant, D. A., Liu, Z. F., Li, T., Zhao, F. Q., Costas, A. M. G., Klatt, C. G., & Overmann, J. (2012). Comparative and functional genomics of anoxygenic green bacteria from the taxa Chlorobi, Chloroflexi, and Acidobacteria. *Functional Genomics and Evolution of Photosynthetic Systems*, *33*, 47–102.

Calvin, M., & Benson, A. A. (1948). The path of carbon in photosynthesis. *Science*, *107*, 476–480.

Campbell, B. J., Engel, A. S., Porter, M. L., & Takai, K. (2006). The versatile epsilon-proteobacteria: Key players in sulphidic habitats. *Nature Reviews Microbiology*, *4*, 458–468.

Canfield, D. E. (1998). A new model for Proterozoic ocean chemistry. *Nature*, *396*, 450–453.

Cassar, N., & Laws, E. A. (2007). Potential contribution of β-carboxylases to photosynthetic carbon isotope fractionation in a marine diatom. *Phycologia*, *46*, 307–314.

Chen, Z.-H., Walker, R. P., Acheson, R. M., & Leegood, R. C. (2002). Phosphoenolpyruvate carboxykinase assayed at physiological concentrations of metal ions has a high affinity for CO_2. *Plant Physiology*, *128*, 160–164.

Close, H. G., Bovee, R., & Pearson, A. (2011). Inverse carbon isotope patterns of lipids and kerogen record heterogeneous primary biomass. *Geobiology*, *9*, 250–265.

Close, H. G., Wakeham, S. G., & Pearson, A. (2014). Lipid and ^{13}C signatures of submicron and suspended particulate organic matter in the Eastern Tropical North Pacific: Implications for the contribution of Bacteria. *Deep Sea Research Part I: Oceanographic Research Papers*, *85*, 15–34.

Damste, J. S. S., & Schouten, S. (1997). Is there evidence for a substantial contribution of prokaryotic biomass to organic carbon in Phanerozoic carbonaceous sediments? *Organic Geochemistry*, *26*, 517–530.

Deniro, M. J., & Epstein, S. (1977). Mechanism of carbon isotope fractionation associated with lipid synthesis. *Science*, *197*, 261–263.

Deniro, M. J., & Epstein, S. (1978). Influence of diet on distribution of carbon isotopes in animals. *Geochimica et Cosmochimica Acta*, *42*, 495–506.

Des Marais, D. J., Strauss, H., Summons, R. E., & Hayes, J. M. (1992). Carbon isotope evidence for the stepwise oxidation of the proterozoic environment. *Nature*, *359*, 605–609.

Evans, M. C. W., Buchanan, B. B., & Arnon, D. I. (1966). A new ferredoxin-dependent carbon reduction cycle in a photosynthetic bacterium. *Proceedings of the National Academy of Sciences of the United States of America*, *55*, 928–934.

French, K. L., Rocher, D., Zumberge, J. E., & Summons, R. E. (2015). Assessing the distribution of sedimentary C-40 carotenoids through time. *Geobiology*, *13*, 139–151.

French, K. L., Sepulveda, J., Trabucho-Alexandre, J., Groceke, D. R., & Summons, R. E. (2014). Organic geochemistry of the early Toarcian oceanic anoxic event in Hawsker Bottoms, Yorkshire, England. *Earth and Planetary Science Letters*, *390*, 116–127.

Grice, K., Cao, C. Q., Love, G. D., Bottcher, M. E., Twitchett, R. J., Grosjean, E., & Jin, Y. G. (2005). Photic zone euxinia during the Permian-Triassic superanoxic event. *Science*, *307*, 706–709.

Grice, K., Schaeffer, P., Schwark, L., & Maxwell, J. R. (1996). Molecular indicators of palaeoenvironmental conditions in an immature Permian shale (Kupferschiefer, Lower Rhine Basin, north-west Germany) from free and S-bound lipids. *Organic Geochemistry*, *25*, 131–147.

Guthrie, J. M. (1996). Molecular and carbon isotopic analysis of individual biological markers: Evidence for sources of organic matter and paleoenvironmental conditions in the Upper Ordovician Maquoketa Group, Illinois Basin, USA. *Organic Geochemistry*, *25*, 439–460.

Guy, R. D., Fogel, M. L., & Berry, J. A. (1993). Photosynthetic fractionation of the stable isotopes of oxygen and carbon. *Plant Physiology*, *101*, 37–47.

Hanson, T. E., Alber, B. E., & Tabita, F. R. (2012). Phototrophic CO_2 Fixation: Recent insights into ancient metabolisms. *Functional Genomics and Evolution of Photosynthetic Systems*, *33*, 225–251.

Hayes, J. M. (2001). Fractionation of carbon and hydrogen isotopes in biosynthetic processes. *Reviews in Mineralogy and Geochemistry*, *43*, 225–277.

Hayes, J. M., Strauss, H., & Kaufman, A. J. (1999). The abundance of C-13 in marine organic matter and isotopic fractionation in the global biogeochemical cycle of carbon during the past 800 Ma. *Chemical Geology*, *161*, 103–125.

Imhoff, J. F.(2005). Family I. Chromatiaceae Bavendamm 1924, 125^{AL} emend. Imhoff 1984b, 339. In D. J. Brenner, N. R. Krieg, J. T. Staley & G. M. Garrity (Eds.), *Bergey's manual of systematic bacteriology* (pp. 3–40). New York, NY: Springer.

Imhoff, J. F., & Bias-Imhoff, U. (1995). Lipids, quinones and fatty acids of anoxygenic phototrophic bacteria. In R. E. Blankenship, M. T. Madigan & C. E. Bauer (Eds.), *Anoxygenic photosynthetic bacteria* (pp. 179–205). Dordrecht, The Netherlands: Springer. ISBN 978-0-7923-3681-5.

Jahnke, L. L., Embaye, T., Hope, J., Turk, K. A., Van Zuilen, M., Des Marais, D. J., & Summons, R. E. (2004). Lipid biomarker and carbon isotopic signatures for stromatolite-forming, microbial mat communities and Phormidium cultures from Yellowstone National Park. *Geobiology*, *2*, 31–47.

Joachimski, M. M., Ostertag-Henning, C., Pancost, R. D., Strauss, H., Freeman, K. H., Littke, R., & Racki, G. (2001). Water column anoxia, enhanced productivity and concomitant changes in delta C-13 and delta S-34 across the Frasnian-Famennian boundary (Kowala Holy Cross Mountains/Poland). *Chemical Geology*, *175*, 109–131.

Johnston, D. T., Poulton, S. W., Dehler, C., Porter, S., Husson, J., Canfield, D. E., & Knoll, A. H. (2010). An emerging picture of Neoproterozoic ocean chemistry: Insights from the Chuar Group, Grand Canyon, USA. *Earth and Planetary Science Letters*, *290*, 64–73.

Johnston, D. T., Wolfe-Simon, F., Pearson, A., & Knoll, A. H. (2009). Anoxygenic photosynthesis modulated Proterozoic oxygen and

sustained Earth's middle age. *Proceedings of the National Academy of Sciences of the United States of America*, *106*, 16925–16929.

Kampf, C., & Pfennig, N. (1980). Capacity of chromatiaceae for chemotrophic growth. Specific respiration rates of *Thiocystis violacea* and *Chromatium vinosum*. *Archives of Microbiology*, *127*, 125–135.

Kelly, A. E., Love, G. D., Zumberge, J. E., & Summons, R. E. (2011). Hydrocarbon biomarkers of Neoproterozoic to Lower Cambrian oils from eastern Siberia. *Organic Geochemistry*, *42*, 640–654.

Larsen, T., Taylor, D. L., Leigh, M. B., & Brien, D. M. O. (2009). Stable isotope fingerprinting: A novel method for identifying plant, fungal, or bacterial origins of amino acids. *Ecology*, *90*, 3526–3535.

Leegood, R. C., & Walker, R. P. (2003). Regulation and roles of phosphoenolpyruvate carboxykinase in plants. *Archives of Biochemistry and Biophysics*, *414*, 204–210.

Lichtenthaler, H. K., Rohmer, M., & Schwender, J. (1997). Two independent biochemical pathways for isopentenyl diphosphate and isoprenoid biosynthesis in higher plants. *Physiologia Plantarum*, *101*, 643–652.

Logan, G. A., Hayes, J. M., Hieshima, G. B., & Summons, R. E. (1995). Terminal Proterozoic reorganization of biogeochemical cycles. *Nature*, *376*, 53–56.

Logan, G. A., Summons, R. E., & Hayes, J. M. (1997). An isotopic biogeochemical study of neoproterozoic and early Cambrian sediments from the Centralian Superbasin, Australia. *Geochimica et Cosmochimica Acta*, *61*, 5391–5409.

Lombard, J., & Moreira, D. (2011). Origins and early evolution of the mevalonate pathway of isoprenoid biosynthesis in the three domains of life. *Molecular Biology and Evolution*, *28*, 87–99.

Luo, G. M., Algeo, T. J., Huang, J. H., Zhou, W. F., Wang, Y. B., Yang, H., & Xie, S. C. (2014). Vertical delta C-13(org) gradients record changes in planktonic microbial community composition during the end-Permian mass extinction. *Palaeogeography Palaeoclimatology Palaeoecology*, *396*, 119–131.

Macko, S. A., Fogel, M. L., Hare, P. E., & Hoering, T. C. (1987). Isotopic fractionation of nitrogen and carbon in the synthesis of amino acids by microorganisms. *Chemical Geology*, *65*, 79–92.

Madigan, M. T., & Jung, D. O. (2009). The purple phototrophic bacteria. In C. N. Hunter, F. Daldal, M. C. Thurnauer & J. T. Beatty (Eds.), *Advances in photosynthesis and respiration—An overview of purple bacteria, systematics, physiology, and habitats* (Vol. *28*, pp. 1–15). Dordrecht, The Netherlands: Springer.

Madigan, M. T., Takigiku, R., Lee, R. G., Gest, H., & Hayes, J. M. (1989). Carbon isotope fractionation by thermophilic phototrophic sulfur bacteria—Evidence for autotrophic growth in natural populations. *Applied and Environmental Microbiology*, *55*, 639–644.

Melzer, E., & Schmidt, H.-L. (1987). Carbon isotope effects on the pyruvate dehydrogenase reaction and their importance for relative carbon-13 depletion in lipids. *Journal of Biological Chemistry*, *262*, 8159–8164.

Meyer, K. M., & Kump, L. R. (2008). Oceanic euxinia in Earth history: Causes and consequences. *Annual Review of Earth and Planetary Sciences*, *36*, 251–288.

Meyer, K. M., Macalady, J. L., Fulton, J. M., Kump, L. R., Schaperdoth, I., & Freeman, K. H. (2011). Carotenoid biomarkers as an imperfect reflection of the anoxygenic phototrophic community in meromictic Fayetteville Green Lake. *Geobiology*, *9*, 321–329.

Michelou, V. K., Cottrell, M. T., & Kirchman, D. L. (2007). Light-stimulated bacterial production and amino acid assimilation by cyanobacteria and other microbes in the North Atlantic Ocean. *Applied and Environmental Microbiology*, *73*, 5539–5546.

Mohr, W., Tang, T., Sattin, S. R., Bovee, R. J., & Pearson, A. (2014). Protein stable isotope fingerprinting: Multidimensional protein chromatography coupled to stable isotope-ratio mass spectrometry. *Analytical Chemistry*, *86*, 8514–8520.

Monson, K. D., & Hayes, J. M. (1982). Carbon isotopic fractionation in the biosynthesis of bacterial fatty acids—Ozonolysis of unsaturated fatty acids as a means of determining the intramolecular distribution of carbon isotopes. *Geochimica et Cosmochimica Acta*, *46*, 139–149.

Nabbefeld, B., Grice, K., Twitchett, R. J., Summons, R. E., Hays, L., Bottcher, M. E., & Asif, M. (2010). An integrated biomarker, isotopic and palaeoenvironmental study through the Late Permian event at Lusitaniadalen, Spitsbergen. *Earth and Planetary Science Letters*, *291*, 84–96.

Nold, S., & Ward, D. (1996). Photosynthate partitioning and fermentation in hot spring microbial mat communities. *Applied and Environmental Microbiology*, *62*, 4598–4607.

O'Leary, M. H., Rife, J. E., & Slater, J. D. (1981). Kinetic and isotope effect studies of maize phosphoenolpyruvate carboxylase. *Biochemistry*, *20*, 7308–7314.

Overmann, J., Beatty, J. T., Hall, K. J., Pfennig, N., & Northcote, T. G. (1991). Characterization of a dense, purple sulfur bacterial layer in a meromictic salt lake. *Limnology and Oceanography*, *36*, 846–859.

Pagés, A., Grice, K., Ertefai, T., Skrzypek, G., Jahnert, R., & Greenwood, P. (2014). Organic geochemical studies of modern microbial mats from Shark Bay: Part 1: Influence of depth and salinity on lipid biomarkers and their isotopic biosignatures. *Geobiology*, *12*, 469–487.

Pancost, R. D., Crawford, N., Magness, S., Turner, A., Jenkyns, H. C., & Maxwell, J. R. (2004). Further evidence for the development of photic-zone euxinic conditions during Mesozoic oceanic anoxic events. *Journal of the Geological Society*, *161*, 353–364.

Pawlowska, M. M., Butterfield, N. J., & Brocks, J. J. (2012). Lipid taphonomy in the Proterozoic and the effect of microbial mats on biomarker preservation. *Geology*, *41*, 103–106.

Pearson, A., Kraunz, K. S., Dekas, A. E., Sessions, A. L., Leavitt, W. D., & Edwards, K. J. (2008). Quantifying microbial degradation of petroleum hydrocarbons in salt-marsh sediments using the ^{13}C content of bacterial rRNA. *Applied and Environmental Microbiology*, *74*, 1157–1166.

Pearson, A., Sessions, A. L., Edwards, K. J., & Hayes, J. M. (2004). Phylogenetically-specific separation of rRNA from prokaryotes for isotopic analysis. *Marine Chemistry*, *92*, 295–306.

Quandt, L., Gottschalk, G., Ziegler, H., & Stichler, W. (1977). Isotope discrimination by photosynthetic bacteria. *FEMS Microbiology Letters*, *1*, 125–128.

Raven, J. A., & Beardall, J. (2015). The ins and outs of CO_2. *Journal of Experimental Botany*, *67*, 1–13.

Reinfelder, J. R. (2011). Carbon concentrating mechanisms in eukaryotic marine phytoplankton. *Annual Review of Marine Science*, *3*, 291–315.

Rohmer, M., Knani, M., Simonin, P., Sutter, B., & Sahm, H. (1993). Isoprenoid biosynthesis in bacteria—A novel pathway for the early steps leading to isopentenyl diphosphate. *Biochemical Journal*, *295*, 517–524.

Sakata, S., Hayes, J. M., McTaggart, A. R., Evans, R. A., Leckrone, K. J., & Togasaki, R. K. (1997). Carbon isotopic fractionation associated with lipid biosynthesis by a cyanobacterium: Relevance for interpretation of biomarker records. *Geochimica et Cosmochimica Acta*, *61*, 5379–5389.

Schouten, S., Breteler, W., Blokker, P., Schogt, N., Rijpstra, W. I. C., Grice, K., & Damste, J. S. S. (1998). Biosynthetic effects on the stable carbon isotopic compositions of algal lipids: Implications for deciphering the carbon isotopic biomarker record. *Geochimica et Cosmochimica Acta*, *62*, 1397–1406.

Schouten, S., Özdirekcan, S., Van Der Meer, M. T. J., Blokker, P., Baas, M., Hayes, J. M., & Damste, J. S. S. (2008). Evidence for substantial intramolecular heterogeneity in the stable carbon isotopic composition of phytol in photoautotrophic organisms. *Organic Geochemistry*, *39*, 135–146.

Schunck, H., Lavik, G., Desai, D. K., Grosskopf, T., Kalvelage, T., Loscher, C. R., & Laroche, J. (2013). Giant hydrogen sulfide plume in the oxygen minimum zone off Peru supports chemolithoautotrophy. *PLoS One*, *8*(8), e68661.

Schwab, V., & Spangenberg, J. E. (2004). Organic geochemistry across the Permian-Triassic transition at the Idrijca Valley, Western Slovenia. *Applied Geochemistry*, *19*, 55–72.

Scott, K. M., Henn-Sax, M., Harmer, T. L., Longo, D. L., Frame, C. H., & Cavanaugh, C. M. (2007). Kinetic isotope effect and biochemical characterization of form IA RubisCO from the marine cyanobacterium

Prochlorococcus marinus MIT9313. *Limnology and Oceanography*, *52*, 2199–2204.

Scott, J. H., O'Brien, D. M., Emerson, D., Sun, H., McDonald, G. D., Salgado, A., & Fogel, M. L. (2006). An examination of the carbon isotope effects associated with amino acid biosynthesis. *Astrobiology*, *6*, 867–880.

Sessions, A. L., Sylva, S. P., & Hayes, J. M. (2005). Moving-wire device for carbon isotopic analyses of nanogram quantities of nonvolatille organic carbon. *Analytical Chemistry*, *77*, 6519–6527.

Silfer, J. A., Engel, M. H., Macko, S. A., & Jumeau, E. J. (1991). Stable carbon isotope analysis of amino acid enantiomers by conventional isotope ratio mass spectrometry and combined gas chromatography—Isotope ratio mass spectrometry. *Analytical Chemistry*, *63*, 370–374.

Tang, K. H., Feng, X., Tang, Y. J., & Blankenship, R. E. (2009). Carbohydrate metabolism and carbon fixation in *Roseobacter denitrificans* OCh114. *PLoS One*, *4*, e7233. doi:10.1371/journal.pone.0007233

Tang, K. H., Tang, Y. J., & Blankenship, R. E. (2011). Carbon metabolic pathways in phototrophic bacteria and their broader evolutionary implications. *Frontiers in Microbiology*, *2*, 165. doi:10.3389/fmicb.2011.00165

Teece, M. A., Fogel, M. L., Dollhopf, M. E., & Nealson, K. H. (1999). Isotopic fractionation associated with biosynthesis of fatty acids by a marine bacterium under oxic and anoxic conditions. *Organic Geochemistry*, *30*, 1571–1579.

Urbina, J. A., & Avilan, L. (1989). The kinetic mechanism of phosphoenolpyruvate carboxykinase from *Panicum maximum*. *Phytochemistry*, *28*, 1349–1353.

Van Der Meer, M. T. J., Schouten, S., & Damste, J. S. S. (1998). The effect of the reversed tricarboxylic acid cycle on the C-13 contents of bacterial lipids. *Organic Geochemistry*, *28*, 527–533.

Van Der Meer, M. T. J., Schouten, S., Van Dongen, D. E., Rijpstra, W. I. C., Fuchs, G., Damste, J. S. S., & Ward, D. M. (2001). Biosynthetic controls an the C-13 contents of organic components in the photoautotrophic bacterium *Chloroflexus aurantiacus*. *Journal of Biological Chemistry*, *276*, 10971–10976.

Van Der Meer, M. T. J., Schouten, S., De Leeuw, J. W., & Ward, D. M. (2000). Autotrophy of green non-sulphur bacteria in hot spring microbial mats: Biological explanations for isotopically heavy organic carbon in the geological record. *Environmental Microbiology*, *2*, 428–435.

Viale, A. M., Kobayashi, H., & Akazawa, T. (1989). Expressed genes for plant-type ribulose 1,5-bisphosphate carboxylase/oxygenase in the photosynthetic bacterium *Chromatium vinosum*, which possesses two complete sets of the genes. *Journal of Bacteriology*, *171*, 2391–2400.

Voorhies, A. A., Biddanda, B. A., Kendall, S. T., Jain, S., Marcus, D. N., Nold, S. C., & Dick, G. J. (2012). Cyanobacterial life at low O_2: Community genomics and function reveal metabolic versatility and extremely low diversity in a Great Lakes sinkhole mat. *Geobiology*, *10*, 250–267.

Weissgerber, T., Sylvester, M., Kroninger, L., & Dahl, C. (2014). A comparative quantitative proteomic study identifies new proteins relevant for sulfur oxidation in the purple sulfur bacterium *Allochromatium vinosum*. *Applied and Environmental Microbiology*, *80*, 2279–2292.

Weissgerber, T., Watanabe, M., Hoefgen, R., & Dahl, C. (2014). Metabolomic profiling of the purple sulfur bacterium *Allochromatium vinosum* during growth on different reduced sulfur compounds and malate. *Metabolomics*, *10*, 1094–1112.

Weissgerber, T., Zigann, R., Bruce, D., Chang, Y. J., Detter, J. C., Han, C., & Dahl, C. (2011). Complete genome sequence of *Allochromatium vinosum* DSM 180$^{(T)}$. *Standards in Genomic Sciences*, *5*, 311–330.

Yang, C., Hua, Q., & Shimizu, K. (2002). Metabolic flux analysis in *Synechocystis* using isotope distribution from ^{13}C-labeled glucose. *Metabolic Engineering*, *4*, 202–216.

Young, J. D., Shastri, A. A., Stephanopoulos, G., & Morgan, J. A. (2011). Mapping photoautotrophic metabolism with isotopically nonstationary ^{13}C flux analysis. *Metabolic Engineering*, *13*, 656–665.

SUPPORTING INFORMATION

Additional Supporting Information may be found online in the supporting information tab for this article.

How to cite this article: Tang T, Mohr W, Sattin SR, Rogers DR, Girguis PR, and Pearson A. Geochemically distinct carbon isotope distributions in *Allochromatium vinosum* DSM 180^T grown photoautotrophically and photoheterotrophically. *Geobiology*. 2016;00:1–16. doi:10.1111/gbi.12221.